Enhanced methane monitoring: A globally harmonized daily 0.1° XCH_4 through machine learning-based fusion of GOSAT, GOSAT-2, and TROPOMI

Jebun Naher Keya[1,★], Yejin Kim[1,★], Hyunyoung Choi[1], Jungho Im[1,2,3,4,*]

[1]Department of Civil, Urban, Earth, & Environmental Engineering, Ulsan National Institute of Science and Technology, Ulsan, 44919, Republic of Korea
[2]Graduate School of Carbon Neutrality, Ulsan National Institute of Science and Technology, Ulsan, 44919, Republic of Korea
[3]Artificial Intelligence Graduate School, Ulsan National Institute of Science and Technology, Ulsan, 44919, Republic of Korea
[4]Department of Environmental Resources Engineering, State University of New York College of Environmental Science and Forestry, Syracuse, NY 13210, USA

*Corresponding Author: Jungho Im (ersgis@unist.ac.kr)

★These authors contributed equally to this work.

Supplementary

Equations S1–S3 (Statistical Metrics for Model Performance Evaluation)

Model performance was evaluated using four standard statistical metrics: coefficient of determination (R^2; Eq.1), root mean square error (RMSE; Eq. 2), mean bias error (MBE; Eq. 3) and mean absolute error (MAE; Eq.4).

$$R^2 = 1 - \frac{\sum_i (y_i - \hat{y}_i)^2}{\sum_i (y_i - \bar{y})^2} \quad (1)$$

$$RMSE = \sqrt{\frac{1}{n}\sum_{i=1}^{n} (\hat{y}_i - y_i)^2} \quad (2)$$

$$MAE = \frac{1}{n}\sum_{i=1}^{n} |\hat{y}_i - y_i| \quad (3)$$

In the equation, $\hat{y}_i$ represents the predicted value, y_i is observed value, $\bar{y}$ is the mean of observed values, and n is the total number of samples

Table S1. TCCON (GGG2020 version) sites used for evaluation of satellite XCH_4 and machine learning based bias correction.

TCCON site	Latitude, Longitude (°)	Elevation (m)	Data reference
Bremen[a, b]	53.10, 8.85	30	Notholt et al., 2022
Burgos	18.53, 120.65	35	Morino et al., 2022
Darwin	12.46, 130.93	37	Deutscher et al., 2023
East Trout Lake	54.35, -104.99	501.8	Wunch et al., 2022
Edwards[c]	34.96, -117.88	888	Iraci et al., 2022
Garmisch[c]	47.48, 11.06	743	Sussmann et al., 2025
Hefei	31.90, 117.17	30	Liu et al., 2023
Karlsruhe	49.10, 8.44	119	Hase et al., 2024
Lamont	36.60, -97.49	320	Wennberg et al., 2025
Lauder	-45.04, 169.68	370	Pollard et al., 2022
Nicosia[a]	35.14, 33.38	185	Petri et al., 2024
Orléans	47.97, 2.11	130	Warneke et al., 2024
Paris	48.85, 2.36	60	Té et al., 2022
Park Falls	45.95, -90.27	442	Wennberg et al., 2022
Pasadena	34.14, -118.13	210	Wennberg et al., 2022
Rikubetsu[a]	43.46, 143.77	380	Morino et al., 2022
Saga	33.24, 130.29	7	Shiomi et al., 2022
Sodankylä	67.37, 26.63	188	Kivi et al., 2022
Tsukuba	36.05, 140.12	31	Morino et al., 2022
Xianghe[c]	39.75, 116.96	36	Zhou et al., 2022

[a] Sites excluded from the GOSAT evaluation under the GOSAT colocation criteria. [b] Sites excluded from the GOSAT-2 evaluation under the GOSAT-2 colocation criteria. [c] Independent test sites not used for training/validation of the machine learning based bias-correction model.

Table S2. GOSAT XCH_4 retrieval parameters used to estimate Δ(GOSAT - TCCON).

GOSAT predictor variables	**Units**
1. Bias corrected XCO_2 retrieved	ppb
1. Aerosol Optical Thickness (AOT1 & 2)	-
2. Cirrus Optical Thickness	-
3. Longitude	degree
4 Reference CO_2 Profile (total)	ppb
5. Reference CO_2 Profile 1	Mol cm^{-2}
6. Satellite zenith	degree
7. Reference pressure – retrieved pressure (ΔPs)	hPa
8. Temperature shift	K

Table S3. GOSAT-2 XCH_4 retrieval parameters used to estimate Δ(GOSAT-2 - TCCON).

GOSAT-2 predictor variables	**Units**
1. Reference pressure – retrieved pressure (ΔPs)	hPa
2. XCO_2 retrieved	-
3. H_2O Profile uncertainty	ppb
4. Longitude	deg
5. XCH_4 Degrees of Freedom	-
6. Pressure level	hPa
7. Solar Zenith Angle (SZA)	deg
8. Column averaging kernel vertical level 1	-
9. Fluorescent Slope	-
10. Aerosol Optical Thickness Type1 + Type2 (total)	-
11. Residual Chi-Squared : Band 3	-

Table S4. TROPOMI XCH_4 retrieval parameters used to estimate Δ(TROPOMI - TCCON) in step 1 and Δ(TROPOMI – GOSAT-2) in step 2

TROPOMI predictor variables (abbreviation)	**Units**
1. XCH_4 precision	ppb
2. Fluorescence	mol s^{-1} m^{-2} nm^{-1} sr-1
3–4. CO total column and precision	mol m^{-2}
5–6. H_2O total column and precision	mol m^{-2}
7–8. Aerosol size and precision	-
9–10. Aerosol height and precision	m
11–12. Aerosol column and precision	m^{-2}
13–14. NIR surface albedo and precision	-
15–16. SWIR surface albedo and precision	-
17. NIR aerosol optical thickness	-
18. SWIR aerosol optical thickness	-
19. NIR chi-square	-
20. SWIR chi-square	-
22. Solar zenith angle (SOZ)	degree
23. Solar azimuth angle (SOA)	degree
24. Satellite zenith angle (SAZ)	degree
25. Satellite azimuth angle (SAA)	degree
26. Surface altitude	m
27. Surface classification	-
28. U10 wind speed (U10)	m s^{-1}
29. V10 wind speed (V10)	m s^{-1}
30. NIR cirrus reflectance	-
31. SWIR cirrus reflectance	-
32. XCH4 profile a priori	mol m^{-2}

Table S5. GOSAT XCH_4 retrieval parameters used to estimate Δ(GOSAT – GOSAT-2) in Step2

1. Surface pressure	hPa
2. Reference surface pressure	hPa
3. Total column of dry air molecules	Mol cm^{-2}
4. ΔPs : reference pressure – retrieved pressure	hPa
5. Altitude (height)	m
6. Retrieved XCO_2	ppb
7. Bias corrected XCO_2	ppb
8–19. Reference CO_2 profile at pressure levels P4–P15	Mol cm^{-2}
20. Total reference CO_2 profile column	Mol cm^{-2}
21. Vertically integrated CH_4 column	Mol cm^{-2}
22. Aerosol Optical Thickness type-2	-
23. Air mass	-
24–25. Residual mean square	-
26. Column averaging kernel vertical level 6	-

Table S6. Cross-validation results comparing Random Forest (RF) and eXtreme Gradient Boosting (XGBoost) for TROPOMI, GOSAT, and GOSAT-2 bias correction against TCCON. For each metric, the better-performing value between the two algorithms is shown in bold.

		RF			**XGBoost**		
	CV type	LOSOCV[a]	LOMOCV[b]	LOYOCV[c]	LOSOCV	LOMOCV	LOYOCV
TROPOMI	N	5,156					
	R^2	0.78	0.82	0.81	0.79	0.84	0.82
	MAE (ppb)	10.48	9.34	9.39	10.20	8.83	9.17
	RMSE (ppb)	13.94	12.78	12.87	13.58	12.06	12.57
GOSAT	N	702					
	R^2	0.87	0.88	0.86	0.86	0.88	0.86
	MAE (ppb)	8.20	7.66	8.42	8.43	7.72	8.53
	RMSE (ppb)	10.85	10.16	11.09	11.13	10.22	11.19
GOSAT-2	N	1,751					
	R^2	0.88	0.91	0.89	0.88	0.90	0.89
	MAE (ppb)	7.68	7.07	7.45	7.89	7.19	7.67
	RMSE (ppb)	10.96	9.86	10.65	11.22	10.04	10.84

[a] LOSOCV: Leave-One-Site-Out Cross-Validation
[b] LOMOCV: Leave-One-Month-Out Cross-Validation
[c] LOYOCV: Leave-One-Year-Out Cross-Validation

Table S7. Cross-validation results comparing Random Forest (RF), eXtreme Gradient Boosting (XGBoost) and Light Gradient Boosting Machine (LightGBM) for TROPOMI and GOSAT bias correction against best-performing ML-based bias-corrected GOSAT-2. For each metric, the better-performing value between the three algorithms is shown in bold.

		RF			**XGBoost**		
	CV type	LOSOCV[a]	LOMOCV[b]	LOYOCV[c]	LOSOCV	LOMOCV	LOYOCV
TROPOMI	N	183,550					
	R^2	0.86	0.87	0.87	0.91	0.92	0.92
	MAE (ppb)	8.50	8.13	8.18	6.78	6.32	6.59
	RMSE (ppb)	11.18	10.72	10.78	9.07	8.49	8.82
GOSAT	N	32,244					
	R^2	0.91	0.92	0.91	0.92	0.92	0.92
	MAE (ppb)	7.22	7.00	9.94	7.06	6.86	7.11
	RMSE (ppb)	9.80	9.50	7.38	9.56	9.33	9.64

[a] LOSOCV: Leave-One-Site-Out Cross-Validation
[b] LOMOCV: Leave-One-Month-Out Cross-Validation
[c] LOYOCV: Leave-One-Year-Out Cross-Validation

Table S9. Seasonal hemispheric and high-emission zone mean XCH_4 concentrations in 2023. Values represent area-weighted seasonal means and spatial standard deviations indicating spatial variability within each region. Amplitude represents the seasonal range (maximum minus minimum concentration) for each region per season.

Region	MAM (ppb)	JJA (ppb)	SON (ppb)	DJF (ppb)	Amplitude (ppb)
0–40N	1903.71 ± 10.04	1901.18 ± 6.27	1917.13 ± 10.69	1917.68 ± 9.38	16.50
0–80N	1883.22 ± 25.05	1889.30 ± 16.68	1903.46 ± 21.91	1915.36 ± 10.09	32.14
60S–0	1850.66 ± 31.90	1857.43 ± 24.52	1856.62 ± 25.22	1854.55 ± 29.29	6.77

Note- NH: Northern Hemisphere (0–80°N); High-emission zone (0–40°N); SH: Southern Hemisphere (60°S–0°). MAM, JJA, SON, and DJF represent March–May, June–August, September–November, and December–February, respectively.

Figure S1. Spatial cross-validation (SPCV) fold distribution for latitudinal generalization assessment. The bias correction models were evaluated using leave-one-band-out cross-validation (LOBOCV)across eleven latitude-based folds spanning 60°S–80°N.

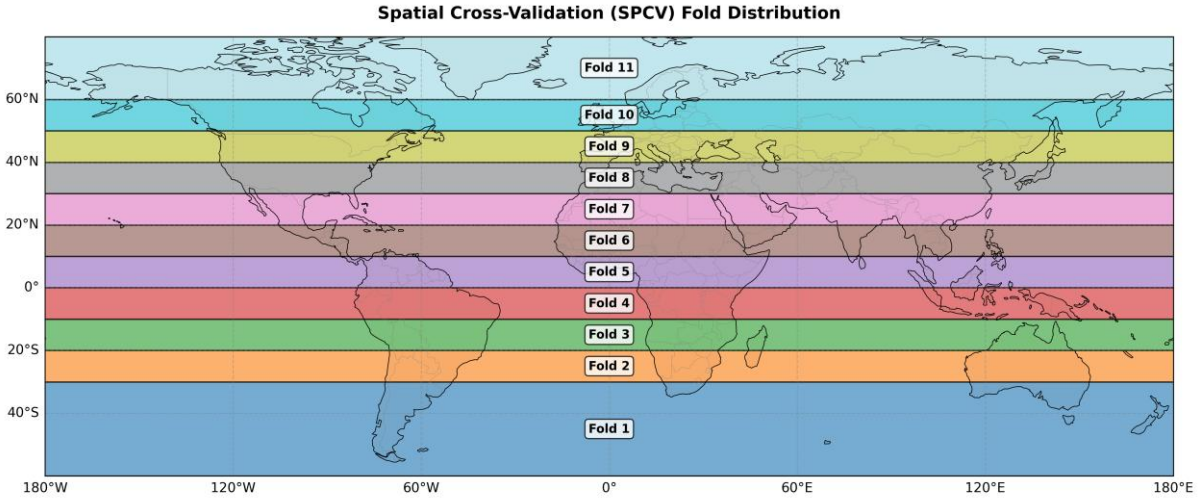

Figure S2. Comparison of operational TROPOMI products (TROPOMI standard and bias correction) and machine-learning based bias correction result (ML Bias correction) with TCCON XCH_4 (GGG2020 version). Shown are the mean (μ) and standard deviation (σ) of the TROPOMI–TCCON XCH4 differences for colocated observations during 2020–2023. Station locations are summarized in Table S1 and mapped in Fig. 1.

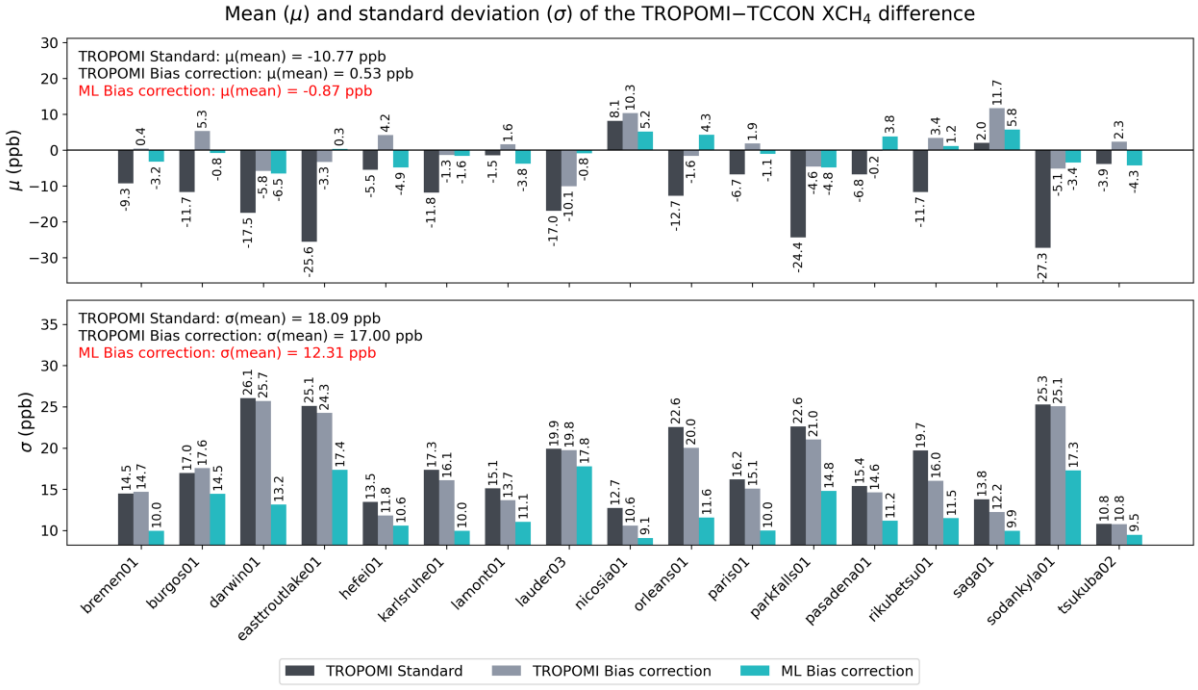

Figure S3. Comparison of operational GOSAT products (GOSAT standard and bias correction) and machine-learning based bias correction result (ML Bias correction) with TCCON XCH_4 (GGG2020 version). Shown are the mean (μ) and standard deviation (σ) of the GOSAT–TCCON XCH_4 differences for colocated observations during 2020–2023. Station locations are summarized in Table S1 and mapped in Fig. 1.

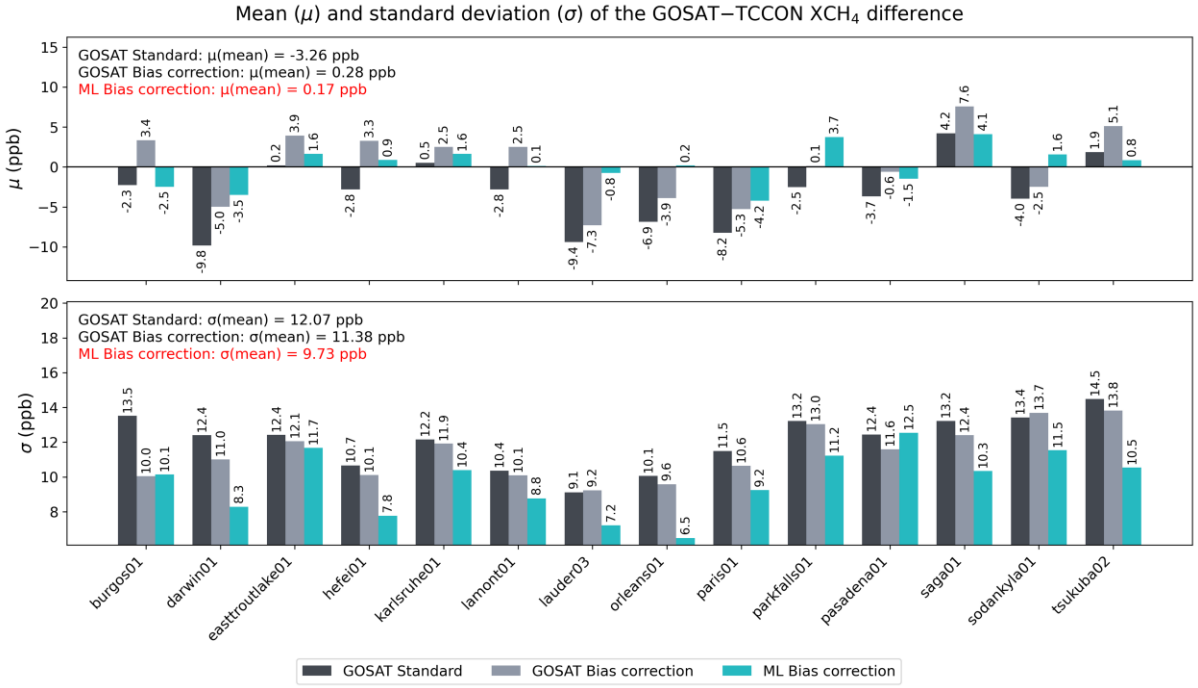

Figure S4. Comparison of operational GOSAT-2 standard product and machine-learning based bias correction result (ML Bias correction) with TCCON XCH_4 (GGG2020 version). Shown are the mean (μ) and standard deviation (σ) of the GOSAT-2–TCCON XCH_4 differences for colocated observations during 2020–2023. Station locations are summarized in Table S1 and mapped in Fig. 1.

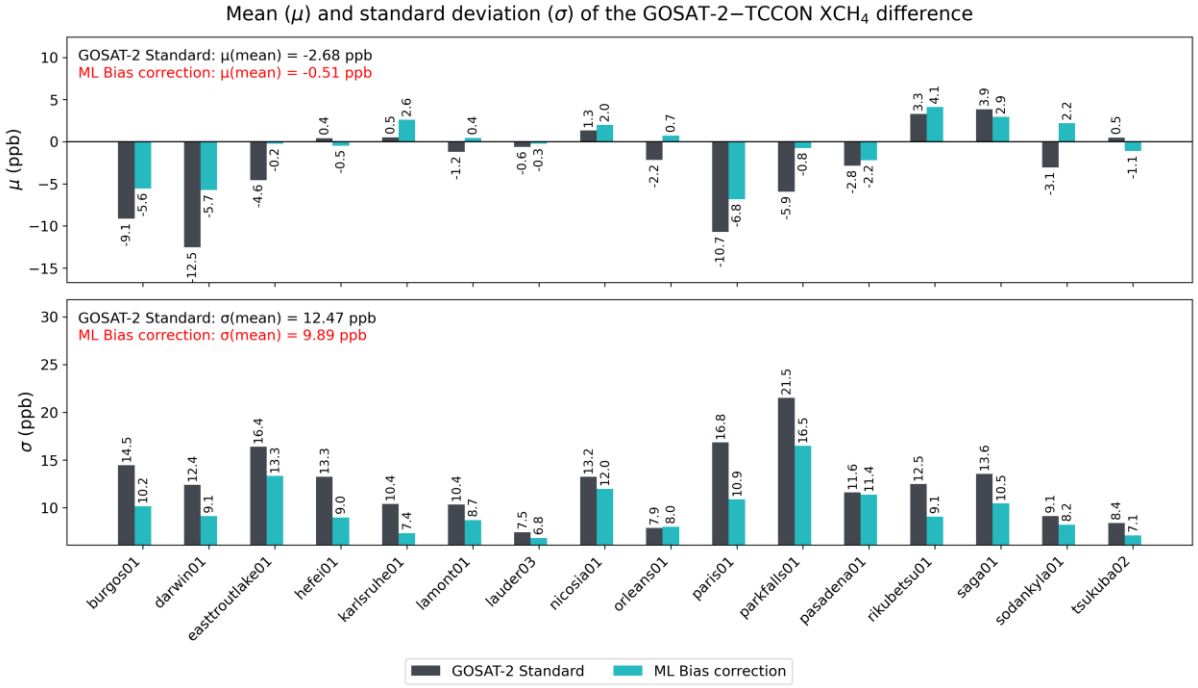

Figure S5. Global coverage comparison between TROPOMI and fused XCH_4 products (2020–2023). (a) Annual global land coverage showing TROPOMI official product (grey) and fused product (green), with percentage improvement indicated for each year. (b) Monthly relative coverage improvement of fused product over TROPOMI for each year from 2020–2023, demonstrating temporal resilience during TROPOMI data gaps in July–August 2022 and August 2023 caused by missing VIIRS cloud screening data.